A Nanoscale Gas State

Xue H. Zhang, Abbas Khan, and William A. Ducker*

Department of Chemical and Biomolecular Engineering, University of Melbourne, Melbourne 3010, Australia

(Received 8 October 2006; published 26 March 2007)

We show that a very thin (5–80 nm) gas phase can exist for a long time (>1 h) at the interface between a hydrophobic solid and water. We create the gas phase from CO_2, which allows us to determine the chemical identity, phase state, and density via infrared spectroscopy. The average density reveals that the gas is at approximately atmospheric pressure, which explains the unexpectedly long lifetime of the gas phase under ambient conditions. The nanoscale gas phase is reproducibly created under conditions where gas solubility is varied.

DOI: 10.1103/PhysRevLett.98.136101 PACS numbers: 68.08.De

The nature of the interface between water and materials that form only weak intermolecular interactions with water (''hydrophobic'' materials) is the subject of intense scrutiny and debate [1–6]. These hydrophobic materials include oil droplets, graphitic materials, many polymers and polymer coatings, air, and some biological surfaces. From a standard assumption of van der Waals and double-layer forces (DLVO theory) [7], it is not possible to accurately predict the stability of an oil emulsion or to understand why there is often a long-range (10–100 nm) attractive force between hydrophobic surfaces [4–6]. Our failure to understand hydrophobic surfaces has evolved into the hypothesis that, in many cases, the interface between hydrophobic materials and water is decorated with nanoscale gas bubbles. The interfacial bubble hypothesis has been used to rationalize the long-ranged hydrophobic force [4–6,8–10] and the unexpected lubrication of hydrophobic surfaces [11] and may also explain the controversial and unexpected emulsification and stability of oil emulsions in degassed water [12]. Some other manifestations of the long-range attraction may be due to the existence of mobile charge patches on the solids [6,13,14].

To date, evidence for the existence of interfacial nanobubbles is inconsistent or indirect. If present, they should be detected by techniques that are sensitive to the high refractive index contrast between water and air (e.g., ellipsometry and x-ray reflectivity) or from neutron reflectivity measurements. Recent evidence from experiments arising from different labs has produced contradictory results [6,15,16], and, in any case, it is difficult to distinguish interfacial bubbles (i.e., discrete compartments of gas) from a continuous layer of water that has a reduced density. Several researchers have observed objects at the interface between water and hydrophobic materials using atomic force microscopy (AFM) that they attributed to air bubbles [5,17,18], but there has never been direct evidence that these objects are gaseous, and there is an ever-present concern that the observed nanostructures are simply contamination [19,20].

The interfacial bubble hypothesis also raises a potential theoretical problem. A simple force balance (the Laplace equation) shows that highly curved bubbles are under a high pressure (e.g., 14 atm for 100 nm radius in water) and, therefore, should collapse in less than 100 ms [21]. So, to remain stable, a nanobubble must have a correspondingly large radius of curvature [17].

Unambiguous evidence of a gas phase is made possible by the recent development of a reproducible method by solvent exchange for obtaining nanostructures that were observed at the interface between water and hydrophobic solids by AFM [22,23]. The method is simply to expose a solid to ethanol and then to water [24]. Ethanol has a greater solubility for most gases, which provides the opportunity for the gas to become supersaturated in the water and, thus, form bubbles on the solid [24]. Our experiment involves three stages, all at 25–27 °C: *Stage one:* We expose a hydrophobized-silicon wafer to CO_2-saturated water. This acts as a control for stage three; it is not required to generate bubbles. *Stage two:* We replace the water with CO_2-saturated ethanol. *Stage three:* We replace the ethanol with CO_2-saturated water. We use CO_2 instead of air because the gaseous and aqueous states of CO_2 exhibit very different infrared spectra [25] owing to the rotational fine structure from CO_2 gas. Therefore, infrared spectroscopy can be used to directly identify the phase state of the nanoscale objects that ''precipitate'' from the solution when the solvent is changed. CO_2 also has the requisite solubility differential between water and ethanol solvents [26].

Solutions are prepared by bubbling 5–10 kPa $CO_{2(g)}$ through ethanol or H_2O or H_2O/D_2O mixtures for about two hours. The final *p*H is 3.8 ± 0.2. Note that, in H_2O/D_2O mixtures, H^+ and D^+ exchange rapidly between molecules so DOH is also present. Ambient CO_2 is prevented from entering the light path (in infrared measurements) by maintaining a purge of high purity nitrogen throughout the experiment. Our model hydrophobic material is silicon wafers (Mitsubishi silicon, America-Mod 2 polished wafers) with an adsorbed layer of octadecyltrimethylchlorosilane, which forms an advancing contact angle of $112 \pm 3°$ and a receding angle of $101 \pm 3°$ with water in air.

AFM imaging in stage one (water) or two (ethanol) always shows a simple interface with no nanostructures [Fig. 1(a)], consistent with earlier work [24] in the absence of CO_2. In stage three (water after ethanol), we observe interfacial structures, with heights in the range 5–80 nm [Fig. 1(b)]. A typical structure has a height of 15 nm, the radius of curvature is ~4 μm, and the width is about 800 nm at the junction with the solid. The interfacial structures are stable for over 1 h. The absence of interfacial structures in stage one is consistent with the formation of bubbles through ''precipitation'' of a supersaturated solution rather than the ubiquitous presence of bubbles at hydrophobic interfaces. This helps to explain the current disagreement in the literature: The presence of bubbles depends on the history of the sample, which has not always been controlled.

Under conditions identical to those used to produce the nanostructures shown in Fig. 1, we have measured the infrared spectrum of the interfacial material in an attenuated total internal reflection (ATR) configuration (Fig. 2). The spectrum shows rotational fine structure that unambiguously demonstrates the presence of gaseous CO_2 at the interface in stage three. We have also examined the IR silicon prism during stage three with high resolution optical microscopy (50× objective, ~1.5 μm resolution): No bubbles are visible. The IR experiment shows that there is a gas phase present, the optical images preclude the existence of gas in macroscale bubbles, and the AFM confirms that nanostructures are present. Together, these experiments under identical conditions demonstrate the existence of nanoscale gas bubbles at the interface.

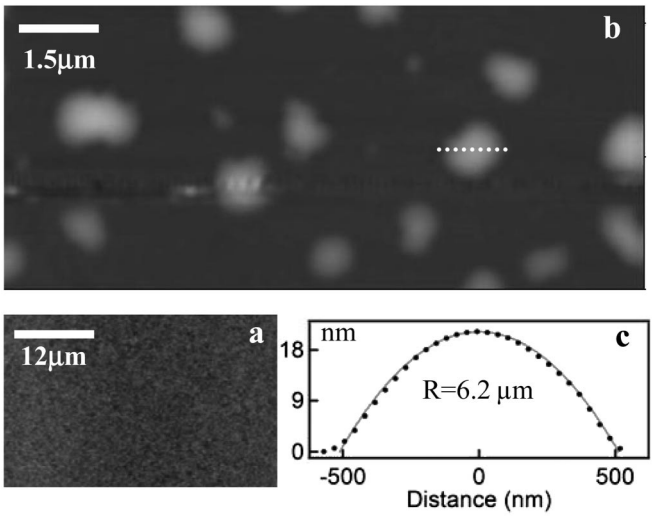

FIG. 1. Tapping-mode AFM images of the interface between hydrophobized silicon and an aqueous CO_2 solution. (a) Stage one (water). The interface is very smooth; the rms roughness is 0.2 nm over 6.25 μm^2. (b) Stage three (after exchange of ethanol for water). (c) Section of the structure marked by the dotted line in (b). The solid line is the best fit to a spherical cap and has a radius of curvature (R) of 6.2 μm (MultiMode Nanoscope IIIa, Veeco, 0.32 N/m or 0.58 N/m spring constants, drive frequency 6–12 kHz).

The key theoretical objection to the presence of interfacial nanobubbles is that, if they are highly curved, they may be under a much higher pressure than the surrounding fluid and, therefore, have a very short lifetime. We can resolve this objection by measuring the pressure of CO_2 gas from the absorbance of the $CO_{2(g)}$. Using a modified version of Beer's law that is applicable to evanescent waves created in the ATR configuration and assuming a two-layer model [27,28]:

$$A^{\mathrm{bub}}_{\mathrm{CO_2}} = N\varepsilon_{\mathrm{co_2}}\rho_{\mathrm{co_2}}d, \quad (1)$$

where A is the absorbance in the CO_2 band, N is the

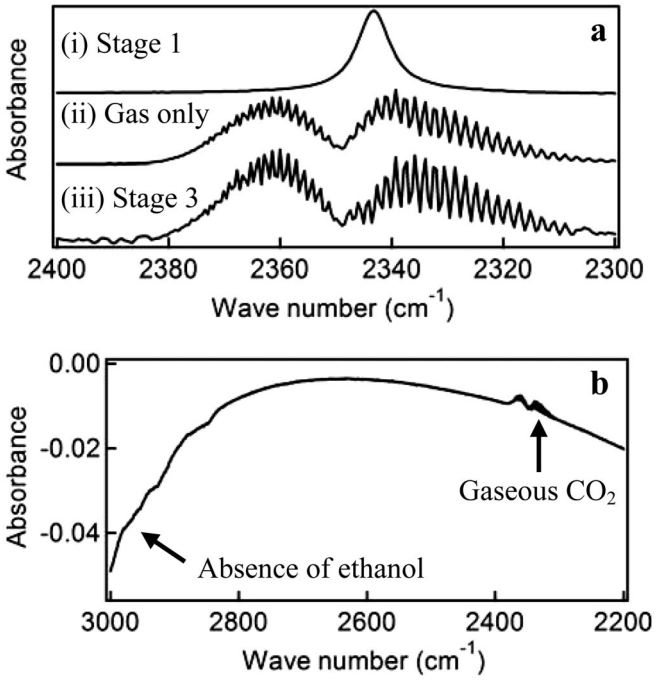

FIG. 2. Fourier transform infrared (FTIR) spectra of the surface of a hydrophobized-silicon prism. All spectra show the difference between the stated conditions and a ''background'' condition. (a) Detail of the CO_2 absorption band. (i) Stage one: CO_2 saturated water. Background spectrum is air-equilibrated water. The spectrum shows the presence of $CO_{2(aq)}$. (The form of dissolved CO_2 in water is mainly $CO_{2(aq)}$ [33].) (ii) $CO_{2(g)}$ spectrum. In a separate experiment, the dry ATR cell is filled with CO_2 gas. Background: Argon. (iii) Stage three. The spectrum shows the presence of $CO_{2(g)}$, as in (ii). Background: Spectrum at stage one. Note that the spectrum differs from (ii) at 2337–2348 cm^{-1} due to a negative aqueous CO_2 band. (b) Same as (a)(iii) but a wider scan demonstrating the absence of ethanol at ~2980 cm^{-1}: The nanostructures are not ethanol. Data were obtained on a Nicolet 5700 FTIR from Thermoelectron Corporation, USA, with a liquid nitrogen cooled mercury-cadmium-telluride detector, incident angles in the range 56°–60°, between 46 and 52 reflections, and a spectrum resolution of 1 cm^{-1}.

number of reflections of the IR beam, ε_{co_2} is the absorption coefficient, ρ_{co_2} is the density of gas in the nanobubbles, and d is the effective path length.

This method requires that we know the effective path length of the infrared radiation through the bubbles. We obtain the effective path length from a repeat of our three stage IR experiment but with a known concentration of water-soluble dye, D_2O (heavy water) in stages one and three. Access of H_2O and D_2O to the evanescent wave is prevented from exactly that portion that contains the CO_2 bubbles. The difference in D_2O absorbance between stages one and three tells us how much of the path length is lost:

$$A_{D_2O} = N\varepsilon_{D_2O}C_{D_2O}d, \quad (2)$$

where C_{D_2O} is the concentration of D_2O solution. ε_{D_2O} is obtained from stage one, using H_2O as the background spectrum. Use of the same d for both estimates is reasonable when the thin intervening films are much thinner than the wavelength of light. A typical bubble has a height of 20 nm, whereas the decay length in water is about 250 nm at 2500 cm^{-1}. If we were to account for the decreased refractive index in the bubble, it would lead to a very slightly shorter path length through the bubble [28] and, therefore, a slightly greater pressure in the bubble, but the validity of this correction is uncertain [28].

Figure 3 shows that after ethanol is replaced by water (stage three) there is a large negative $D_2O_{(aq)}$ band at the same time as a positive $CO_{2(g)}$ band (and a negative $CO_{2(aq)}$ band). The negative D_2O band shows that water has been excluded from the interface, and the positive $CO_{2(g)}$ band shows that gas is at the interface. Using Eqs. (1) and (2) above, we find that the average density of the CO_2 gas is 44 ± 16 mol/m^3. The low density of CO_2 allows us to accurately calculate the pressure from the ideal gas equation; it is 1.1 ± 0.4 atm. Note that, although our error range includes values less than 1 atm, pressures below 1 atm are unreasonable because they require a negative curvature of the bubble.

For comparison, we can calculate the pressure across the bubble surface from the radius of curvature using the Laplace equation. (The pressure inside the bubble is the Laplace pressure plus the ambient pressure of 1 atm.) The radius of curvature of the bubbles, as measured from AFM images, varies in the range 2–45 μm with a typical radius of curvature of $\sim$4 μm. This corresponds to a pressure inside the bubbles in the range 1.7–1.0 atm, with a typical value of 1.4 atm. Because the big bubbles contribute more to the average pressure than the little bubbles, the average pressure will be somewhat lower than suggested by the average radius.

So we have two measures of the pressure that are consistent and that show that the pressure inside the bubble is similar to the pressure of the surrounding liquid (atmospheric). The low pressure explains why the bubbles are at least metastable: The driving force to dissolution from the pressure differential is small. Note that the gas pressure and the pressure obtained from the Laplace equation may differ because the gas film is very thin (typical highest point from the surface: 10–20 nm), so there could be substantial surface forces exerted between the solid-gas and gas-water interfaces.

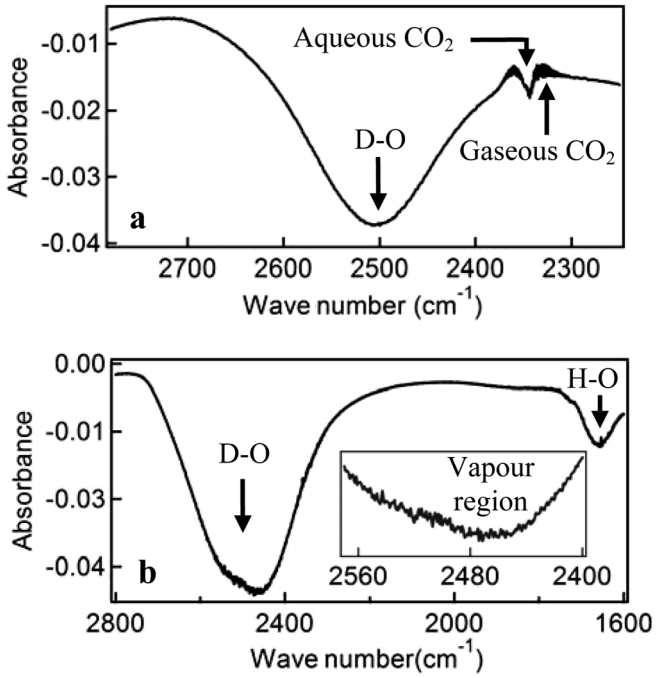

FIG. 3. ATR-FTIR spectra of interface between hydrophobized silicon and a H_2O/D_2O solution in stage three with the spectrum in stage one as the background. (a) 5 vol % D_2O solution saturated with CO_2. There is a large negative O-D band ($\sim$2500 cm^{-1}) due to the exclusion of DOH/D_2O from the silicon-water interface, a negative aqueous CO_2 band ($\sim$2343 cm^{-1}), and a positive gaseous CO_2 band. (b) 30 vol % D_2O solution equilibrated with air. There is fine structure with the same peak positions [29] as in gaseous phase O-D superimposed on the negative band due to absorption by the liquid phase O-D.

So far, we have proven the existence of gas phase CO_2 at the interface. But the bubbles also contain some water vapor. Water vapor shows rotational fine structure in the IR spectrum [29,30], and this is clearly visible in the O-D band in stage three [Fig. 3(b)]. We also observe fine structure in the O-H stretch region, but, because of the very large absorption of infrared radiation by liquid H_2O in this part of the spectrum, it is difficult to distinguish $H_2O_{(g)}$ in interfacial bubbles from ambient $H_2O_{(g)}$ in the IR path length outside the fluid cell. It is reasonable to find gas phase water, because the bubble is in direct contact with the surrounding water. The vapor pressure of water (either H_2O or D_2O) at room temperature is about 0.03 atm [31], so water will make only a small contribution to the total gas pressure in the bubble.

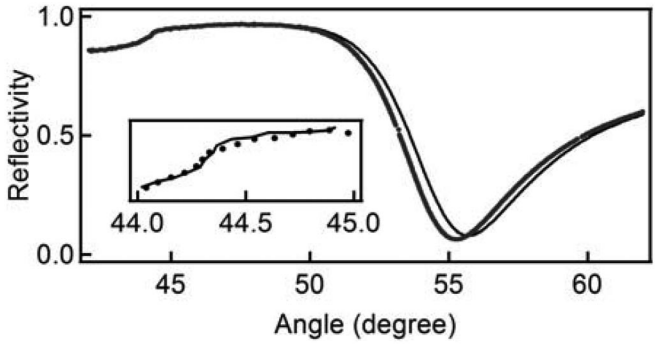

FIG. 4. SPR at the interface between thiol-coated gold film and air-equilibrated water in stages one (thin line) and three (thick line, circles in inset). The critical angles in the two curves are the same (see inset), which indicates that the refractive index of the bulk medium is the same after the exchange. The resonance angle always shifts to a lower angle after the exchange, which demonstrates that a thin layer with a refractive index lower than bulk water has been formed in stage three. The extent of resonance angle shift is not constant from experiment to experiment, suggesting variation in the coverage or size of the bubbles.

We can qualitatively confirm the existence of a low refractive index film at a hydrophobic interface through surface plasmon resonance (SPR, Optrel, Germany) experiments [32]. In these experiments, a 631.6 nm, *p*-polarized laser beam was coupled into a prism (SF10 glass, Schott) in the Kretschmann configuration. These experiments were performed on a gold film coated with a layer of 1-decane thiol. The advancing angle of water on the thiol-coated gold surface was 104°, and the receding angle was 93°. At stage three, the resonance is at a lower angle than at stage one (Fig. 4), which demonstrates the displacement of water (index 1.33) by a lower index material, i.e., consistent with the adsorption of a gaseous phase (refractive index $\sim$1.00).

In summary, we provide unambiguous evidence for the existence of a nanoscale gaseous phase at the hydrophobic solid-water interface. The average pressure in the bubbles is 1.1 ± 0.4 atm, which is consistent with the observed gentle radius of curvature ($R \sim 4$ μm). The small pressure difference across the interface explains why the nanobubbles have such a long lifetime. Our measurements resolve the long-standing debate over whether a nanoscale gas phase can exist at an interface. Work is now underway to determine the stability of a nanobubble-decorated interface.

The presence of the gas phase depends on the previous history of the interface. In some cases, nanobubbles could be used to human advantage; e.g., they could be deliberately generated to lubricate flow in narrow channels, and in some cases care should be taken to avoid their production, e.g., to maintain the stability of emulsions.

This Letter is based on research funded by the Australian Research Council and the NSF Contract No. CHE 0203987. We thank Dr. Anthony Quinn, Dr. Tim Senden, Dr. Nobuo Meada, and Mr. Darwin Lau for valuable assistance.

*To whom all correspondence should be addressed.
Electronic address: wducker@unimelb.edu.au

[1] P. Ball, Nature (London) **423**, 25 (2003).
[2] R. M. M. Smeets *et al.*, Phys. Rev. Lett. **97**, 088101 (2006).
[3] S. M. Dammer and D. Lohse, Phys. Rev. Lett. **96**, 206101 (2006).
[4] H. K. Christenson and P. M. Claesson, Adv. Colloid Interface Sci. **91**, 391 (2001).
[5] P. Attard, Adv. Colloid Interface Sci. **104**, 75 (2003).
[6] E. E. Meyer, K. J. Rosenberg, and J. Israelachvili, Proc. Natl. Acad. Sci. U.S.A. **103**, 15 739 (2006).
[7] E. J. W. Verwey and J. T. G. Overbeek, *Theory of the Stability of Lyophobic Colloids* (Elsevier, New York, 1948).
[8] J. L. Parker, P. M. Claesson, and P. Attard, J. Phys. Chem. **98**, 8468 (1994).
[9] V. S. J. Craig, B. W. Ninham, and R. M. Pashley, Langmuir **15**, 1562 (1999).
[10] T. Koishi *et al.*, Phys. Rev. Lett. **93**, 185701 (2004).
[11] P. G. de Gennes, Langmuir **18**, 3413 (2002).
[12] N. Maeda *et al.*, Langmuir **20**, 3129 (2004).
[13] J. H. Zhang *et al.*, Langmuir **21**, 5831 (2005).
[14] S. Perkin, N. Kampf, and J. Klein, Phys. Rev. Lett. **96**, 038301 (2006).
[15] T. R. Jensen *et al.*, Phys. Rev. Lett. **90**, 086101 (2003).
[16] C. T. McKee and W. A. Ducker, Langmuir **21**, 12 153 (2005).
[17] N. Ishida *et al.*, Langmuir **16**, 6377 (2000).
[18] J. W. Yang *et al.*, J. Phys. Chem. B **107**, 6139 (2003).
[19] D. R. Evans, V. S. J. Craig, and T. J. Senden, Physica (Amsterdam) **A339**, 101 (2004).
[20] Y. S. Seo and S. Satija, Langmuir **22**, 7113 (2006).
[21] S. Ljunggren and J. C. Eriksson, Colloids Surf. A **130**, 151 (1997).
[22] X. H. Zhang *et al.*, Langmuir **20**, 3813 (2004).
[23] X. H. Zhang *et al.*, Langmuir **23**, 1778 (2007).
[24] X. H. Zhang, N. Maeda, and V. S. J. Craig, Langmuir **22**, 5025 (2006).
[25] W. Q. Gong *et al.*, Phys. Chem. Chem. Phys. **1**, 2799 (1999).
[26] D. R. Lide, *CRC Handbook of Chemistry and Physics* (Taylor & Francis, London, 2006), p. 8.
[27] M. J. Citra and P. H. Axelsen, Biophys. J. **71**, 1796 (1996).
[28] W. N. Hansen, in *Advances in Electrochemistry and Electrochemical Engineering*, edited by R. H. Muller (Wiley, New York, 1973), Vol. 9.
[29] N. Gailar and E. K. Plyler, J. Chem. Phys. **24**, 1139 (1956).
[30] Y. Marechal, J. Chem. Phys. **95**, 5565 (1991).
[31] A. H. Harvey and E. W. Lemmon, J. Phys. Chem. Ref. Data **31**, 173 (2002).
[32] W. Knoll, Annu. Rev. Phys. Chem. **49**, 569 (1998).
[33] W. Stumm and J. J. Morgan, *Aquatic Chemistry* (Wiley, New York, 1996).